An Atomic-Level Mechanism for Molybdenum Nitrogenase. Part 1. Reduction of Dinitrogen[†]

Marcus C. Durrant*

Computational Biology Group, John Innes Centre, Norwich Research Park, Colney Lane, Norwich NR4 7UH, United Kingdom

Received February 4, 2002; Revised Manuscript Received August 6, 2002

ABSTRACT: The properties of the Fe and Mo sites of the iron−molybdenum cofactor of nitrogenase with respect to binding and activation of N_2 have been studied by molecular mechanics calculations on the local protein environment and by density functional theory (DFT) calculations on subsections of the cofactor. The DFT calculations indicate that the homocitrate ligand of the cofactor can become monodentate on reduction, allowing N_2 to bind at Mo. In addition, the neighboring Fe atom plays a crucial role in N_2 reduction by stabilizing the initial reduced N_2 species and by facilitating cleavage of the N−N bond. The various possible isomers for partially reduced N_2 intermediates have been compared by DFT, and a detailed model for the reduction of N_2 is developed based on these results, together with chemical precedents and the available biochemical data for nitrogenase.

Nitrogenases are enzymes which catalyze the reduction of dinitrogen to ammonia. The most extensively characterized nitrogenase contains both Mo and Fe and is referred to as Mo nitrogenase; in addition, some organisms have alternative nitrogenases containing Fe and V, or Fe only (*1*). These alternative nitrogenases are inferred to have much in common with Mo nitrogenase in terms of structure, but appear to be less efficient than the latter and are generally only expressed when Mo nitrogenase is unavailable to the organism. Mo nitrogenase consists of two component proteins. The Fe protein (component 2) is a homodimer of ∼60 kDa, contains an Fe_4S_4 cubane and acts as a specific electron donor to the MoFe protein (component 1) (*2*). When dithionite is used as the primary reductant in vitro, electron transfer involves association and dissociation of the two nitrogenase proteins and is accompanied by the hydrolysis of ATP. The MoFe protein is an $\alpha_2\beta_2$ tetramer of ∼230 kDa which contains two unique metal−sulfur clusters. The P-clusters (stoichiometry Fe_8S_7) mediate the supply of electrons to the iron−molybdenum cofactor (FeMoco,[1] stoichiometry $MoFe_7S_9$·homocitrate, Figure 1) (*2*, *3*). A considerable weight of evidence implicates the FeMoco as the site of reduction of N_2 and other substrates, including H^+ (*3*). Detailed spectroscopic studies of ^{57}Fe-enriched FeMoco led to formal resting state valency assignments of $[Mo^{IV}Fe^{III}Fe^{II}_6]$ (*4*) or $[Mo^{IV}Fe^{III}{}_3Fe^{II}{}_4]$ (*5*) and suggested that Mo^{III} is accessed on reduction, while recent theoretical studies have provided additional evidence that $[Mo^{IV}Fe^{III}Fe^{II}_6]$ is the correct alternative (*6*). The production of N_2 by Mo nitrogenase is believed (*1*) to have the limiting stoichiometry shown in reaction 1:

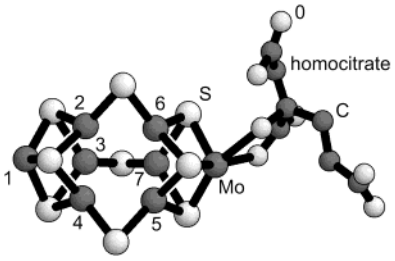

FIGURE 1: FeMoco, showing Fe atom labeling scheme.

$$N_2 + 8H^+ + 8e^- + 16MgATP \rightarrow 2NH_3 + H_2 + 16MgADP + 16P_i \quad (1)$$

Recently, some doubts have been raised over the stoichiometry of the ATP component of reaction 1 following the observation that the Fe protein can be reduced to a stable all-ferrous state, whose crystal structure has been reported (*7*). This form of the Fe protein, if biologically accessible, might be able to transfer two electrons to the MoFe protein for each protein association−dissociation event, halving the catalytic ATP requirement. Recent experimental studies suggest that this is indeed the case (*8*). The stoichiometry of reaction 1 with respect to H_2 follows from the observation that very high pressures of N_2 still result in approximately one H_2 produced per N_2 reduced (*9*). It is not yet clear, however, whether this obligatory hydrogen evolution (OHE) (*10*) is an essential feature of the enzyme's mechanism or merely the consequence of an unavoidable leakage of reducing equivalents during turnover (*3*). Such leakage effects certainly appear to be significant for the alternative nitrogenases; for example, the limiting H_2/N_2 ratio for V nitrogenase is 3.5 (*1*).

[†] Support was provided by the Biotechnology and Biological Sciences Research Council, U.K.

* Corresponding author. Telephone: +44 (0)1603 450704. Fax: +44 (0)1603 450021. E-mail: marcus.durrant@bbsrc.ac.uk

[1] Abbreviations: Av1, Kp1, molybdenum nitrogenases from *A. vinelandii* and *K. pneumoniae*, respectively; DFT, density functional theory; FeMoco, iron−molybdenum cofactor; GS, ground state; MM, molecular mechanics; OHE, obligatory hydrogen evolution.

10.1021/bi025623z CCC: $22.00
Published on Web 10/30/2002

Extensive studies of Mo nitrogenase over several decades have failed to provide definitive information on the atomic mechanism of this enzyme. Nevertheless, these studies have amassed a wealth of experimental data from many different sources. This includes the X-ray crystal structures of the MoFe proteins from *Azotobacter vinelandii* [both the wild-type (*11*) and α-Gln^{195} mutant (*12*)] and from *Klebsiella pneumoniae* (*13*). These resting state structures show the Mo atom of the FeMoco to be chelated by homocitrate and coordinatively saturated, whereas the six central Fe atoms are formally three-coordinate and might therefore be reactive. Together with the discovery of an Fe-only nitrogenase, this has led many to conclude that N_2 fixation probably occurs at one or more of the Fe atoms of the FeMoco, while Mo is present only to "fine-tune" the system. However, an alternative hypothesis that reduction of the MoFe protein allows for opening of the homocitrate chelate ring, thereby allowing a more active role for Mo during catalysis, has also been advanced (*10*, *14*−*16*).

Detailed kinetic analysis of the reduction of N_2 and concomitant production of H_2 by Mo nitrogenase isolated from *K. pneumoniae* revealed several key mechanistic features of these processes, which were used to formulate the Lowe−Thorneley scheme (*17*−*20*) for reduction of N_2. In the Lowe−Thorneley scheme, N_2 fixation occurs over a series of eight redox levels, labeled E_0−E_7. Several of these levels have associated properties such as the ability to bind N_2 and/or release H_2, release of reaction intermediates or products on quenching, and spectroscopic properties, although the degree of characterization tails of markedly for the later redox levels. Meanwhile, extensive genetic and mutagenic studies have provided insights into the effects of the protein on the inorganic components of nitrogenase (*21*), and there is also a very substantial body of model chemistry which is potentially relevant to nitrogenase function. In principle, quantum calculations offer a powerful tool for mapping these chemical data onto the observed biochemistry of nitrogenase, and several research groups have used theoretical methods to study the properties of the FeMoco. However, only methods which properly address key features of transition metal chemistry, such as unpaired electrons and electron correlation effects, have the potential to give meaningful quantitative descriptions of this problem. Density functional theory provides one such approach, and a number of DFT studies of nitrogenase have now been published (*6*, *15*, *16*, *22*−*24*). A severe limitation is the large size of the FeMoco; thus, although a recent DFT study demonstrated that an accurate description of the whole FeMoco can now be achieved (*6*), the challenge of attaining a detailed quantum model of the catalytic properties of the whole cluster remains formidable. An alternative approach is to use simplified FeMoco subsections in DFT calculations; to date, the results of the various published studies do not vary greatly with the nature and size of the model, suggesting that this approximation is valid for qualitative studies. Initial DFT studies of N_2 reduction concentrated on the central Fe atoms of the cluster, in line with the reasoning discussed above. This work has produced a consensus on several important attributes of FeMoco, including the presence of many weak metal−metal bonds within the cluster and the possible significance of low energy distortions for reactivity. Another key observation is that initial binding of N_2 to the central Fe atoms is weak. In perhaps the most thorough DFT study of N_2 binding and reduction published to date, Rod and Nørskov constructed a model for the FeMoco core cluster consisting of an infinite $[MoFe_6S_9]_\infty$ polymer (*23*). They examined a variety of conceivable N_2 binding modes and found that the only stable state with respect to free N_2 was end-on binding to a single Fe atom. The N_2 binding energy ranged from ca. −2 to +5 kcal mol^{-1} depending on the number of H atoms added to the central three sulfurs of the model cluster (0 to 3).

On the basis of experimental observations of the chemistry of FeMoco isolated from the protein, we have suggested a model for nitrogenase action in which the homocitrate ligand becomes monodentate upon reduction of the enzyme, allowing binding of N_2 at Mo (*14*). This model potentially explains the key role of homocitrate in defining the catalytic properties of the enzyme (*21*, *25*−*27*) as well as the observation that detectable N_2 binding occurs only once state E_3 has been reached in the Lowe−Thorneley scheme (*18*). Preliminary DFT studies indicated that binding of N_2 at the Mo site of the FeMoco, although still relatively weak, is nevertheless somewhat stronger than at the trigonal Fe sites and also suggested a functional rationale for the distinctive geometry of the FeMoco in terms of the cleavage of a partially reduced N_2 substrate across a $MoFeS_2$ face of the cluster (*15*). In this paper, the DFT calculations have been extended to explore the feasibility of the homocitrate ring-opening hypothesis in terms of the energetics of this process and to define the properties of the resulting Mo coordination site with respect to N_2 binding and reduction. The results are combined with the findings of a previous analysis of the nitrogenase protein's innate ability to control protonation of both the FeMoco and the N_2 substrate during catalysis (*28*) and the underlying kinetic features of the Lowe−Thorneley scheme to develop an atomic level mechanism for nitrogenase. This is the first reported model in which the properties of the individual states of the Lowe−Thorneley scheme are explained in terms of specific chemical intermediates.

MATERIALS AND METHODS

MM calculations were done with CHEM-X software (*29*). The standard atom parameter set was modified to accommodate the FeMoco by the inclusion of parameters for Fe and Mo, as follows. The connectivity of atoms within the cluster was assumed to be that shown in Figure 1, i.e., metal−metal bonding was ignored. Three- and four-coordinate Fe and six-coordinate Mo atoms were defined, and bond lengths and angles were specified on the basis of the crystal structure geometries (*11*, *13*). All force constants were set to an arbitrary value of 80% of the values for sp^3 C−C and C−C−C bond lengths and angles, respectively. This basic force field reproduced the structure of FeMoco very well. The distortion of FeMoco upon binding N_2 at a trigonal Fe, observed by DFT (*24*), was reproduced reasonably well by specifying the force field S−Fe−N angle as 90°. MM geometry optimizations on FeMoco and its local protein environment were carried out using the protein backbone C and N atoms as a fixed restraint.

All DFT calculations were performed using the B3LYP functional and LanL2DZ basis set as implemented in GAUSSIAN 98W (*30*). Geometry optimizations were carried out using *z*-matrix methods, treating the metal-sulfur section

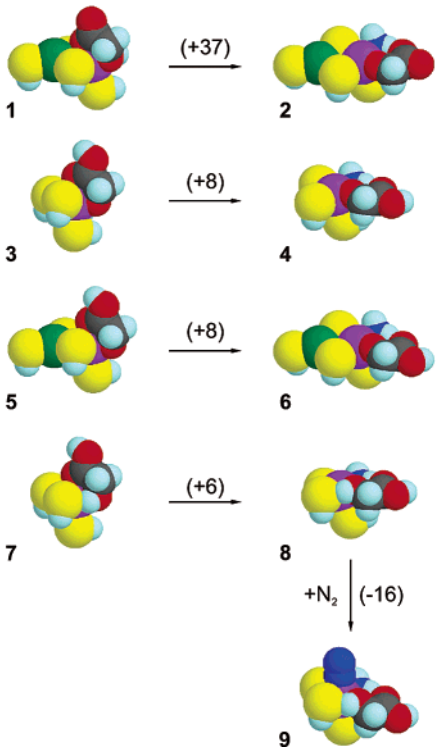

FIGURE 2: Geometry-optimized glycolate structures with relative energies (kcal mol^{-1}) in parentheses. All the Fe atoms are Fe^{II}; the Mo atoms are Mo^{IV} in **1**−**4**, Mo^{III} in **5**−**9**. Color code: C, gray; H, pale blue; N, dark blue; O, red; Fe, green; Mo, purple; S, yellow.

of the models as having a plane of symmetry lying through the Fe and Mo atoms and the terminal SH groups. Because the models used in this work contain only a part of the FeMoco, the metal atoms are relatively unconstrained. In the case of the Fe atom, this resulted in a near-tetrahedral geometry in some cases, e.g., **19** in Figure 3. For the Mo atom, the structural constraints imposed by the rest of the FeMoco were approximated as follows. The angle between the terminal S atom on Mo (S_t) and the plane defined by the Mo and two bridging S atoms was fixed at 109°, and the O and N atoms were constrained to lie in planes defined by fixed S_t-Mo−O and S_t-Mo−N angles of 89° and 88°, respectively. Angle values were taken from the means of those found in the Av1 and Kp1 crystal structures. Initial geometry optimizations were performed on all spin states considered possible, using a subset of variables and the opt = loose convergence option. A final geometry optimization was then carried out on the spin state identified as the lowest in energy, using all variables and full convergence criteria. For some of the calculations on the dinuclear models, the default convergence criteria proved unsatisfactory; after an initial phase in which the energy fell rapidly on each step, there followed a large number of steps in which the energy changed insignificantly. Therefore, for these calculations, geometry optimization was terminated when the change in energy was less than 0.1 kcal mol^{-1} over 10 consecutive optimization minima. Calculations on the extended dinuclear models incorporating the glycolate ligand were restricted to the spin state found to be the ground state in the simpler dinuclear models, using the same geometry optimization protocol.

Protein coordinates were retrieved from the Brookhaven Protein Data Bank (*31*), accession codes 1QGU (Kp1) and 2MIN (Av1). Figures were prepared using RASMOL molecular graphics software (*32*).

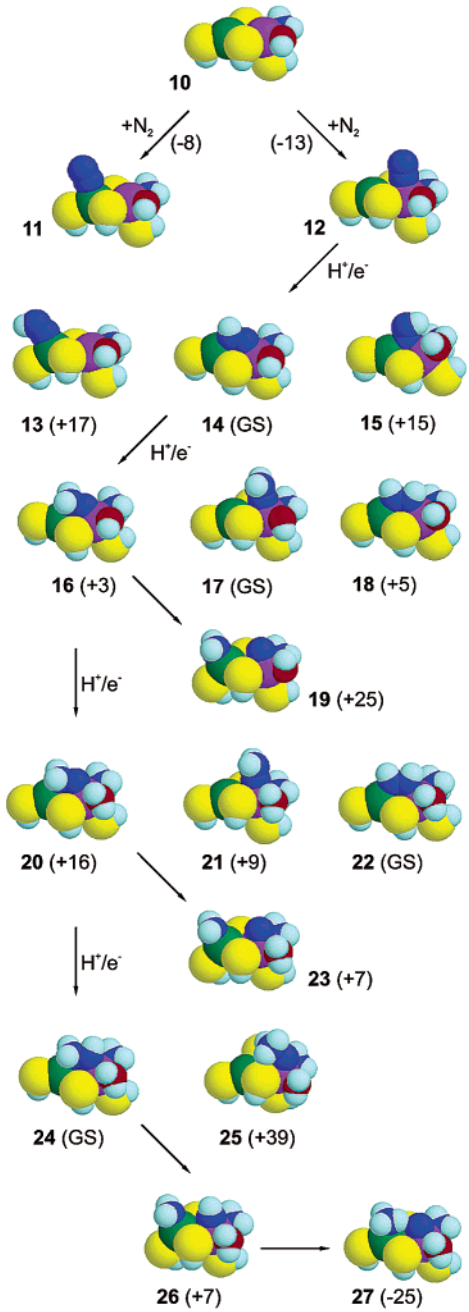

FIGURE 3: Geometry-optimized structures for N_2 binding and reduction. Color code as in Figure 2. Note that in **25**, the N−N bond length was fixed at 1.56 Å (see text).

RESULTS

MM Calculations. As discussed above, the most advanced DFT calculations on the character of N_2 binding to the FeMoco published to date (*24*) indicate that binding of N_2 at Fe is weak, and furthermore that terminal coordination of N_2 to a single Fe center is the only stable mode. In the absence of protein environmental effects, the six central Fe atoms of the FeMoco should display virtually identical affinities for N_2. Therefore, if N_2 does bind at Fe during nitrogenase catalysis, it would be reasonable to expect that one of the six central irons be clearly distinguished from the others. There are two ways in which this could be done.

Table 1: Degree of van der Waals Overlap (%)[a] between N_2 Ligands Attached to the Fe Atoms of FeMoco and the Surrounding Protein[b]

	Av1			Kp1		
atom	raw[c]	opt.[d]	closest residues	raw	opt.	closest residues
Fe2	16	6	His^{195},Ser^{278}	23	3	His^{194}, Ser^{276}
Fe3	10	0	Tyr^{229}	13	0	Tyr^{227}
Fe4	49	−[e]	Gly^{357}, Leu^{358}, Arg^{359}	45	−[e]	Gly^{355},Leu^{356}
Fe5	23	5	Ile^{355}, Gly^{356}, His^{442}	16	5	Met^{353}, Gly^{354}, His^{440}
Fe6	5	0	Gln^{191}, hca	10	0	Gln^{190}, hca
Fe7	7	0	Arg^{96}, hca	0	0	−

[a] Expressed as percentage of van der Waals volume of free N_2 (23.7 $Å^3$). [b] All protein residues are from the α-subunits; hca = homocitrate. [c] Before geometry optimization. [d] After geometry optimization. [e] Failed to give a satisfactory energy-minimized structure.

First, the protein might provide steric protection to five of the sites while leaving the sixth available for N_2 coordination. Second, the protein might exert kinetic control of protonation of N_2 by an efficient proton transfer pathway to a particular Fe site. With these possibilities in mind, the protein environment around the FeMoco in both the Av1 and Kp1 structures has been analyzed. The analysis was done in two ways. First, a completely rigid model taken directly from the crystal structures was used. An N_2 ligand was attached to each of the central Fe atoms of the FeMoco in turn, using fixed Fe−N and N−N bond lengths of 1.81 and 1.15 Å, respectively (taken from the complex $[FeH(N_2)(Me_2PCH_2CH_2PMe_2)_2]^+$, *33*), an Fe−N−N angle of 180°, and coequal S−Fe−N angles. Hydrogen atoms were added to the protein residues in the vicinity of the N_2 ligand, and the degree of overlap between the N_2 and the surrounding protein (excluding waters and the FeMoco) was calculated from the shared van der Waals' volume. The results are given in Table 1. In the second set of calculations, the local geometry around the N_2 ligand was allowed to relax by MM optimization. The protein backbone atoms were kept rigid, and the FeMoco was also treated as a rigid object except for the FeS_3 moiety to which the N_2 was coordinated. The van der Waals overlap of the N_2 ligand was then measured as above.

The results in Table 1 are very consistent for the two different crystal structures. Of the six central Fe atoms, only Fe4 can be clearly ruled out as a potential site for N_2 binding. Fe3, Fe6, and Fe7 can all readily accommodate an N_2 ligand, while Fe2 and Fe5 show only moderate steric hindrance. Considering potential proton transfer groups, here also the Fe atoms are poorly discriminated by the protein. In the case of Kp1, an N_2 on Fe2 is well placed to receive a proton from either α-His^{194} or α-Ser^{276}. Fe3 is served by α-His^{272} and a water (number[2] 56), Fe5 by a water (number 53), Fe6 by homocitrate, and Fe7 by a water (number 10). Of these, previous studies (*28*) have identified α-His^{194} and water number 56 as components of proton relay channels to FeMoco, while water numbers 10 and 53 are associated with the "water pool" (*2*) around homocitrate, which is linked to the protein exterior via a hydrogen bonded chain of water molecules (*28*). Hence, there is a distinct absence of kinetic discrimination in favor of any of the five Fe sites which can accommodate N_2 in terms of the rate of protonation of the

[2] Water numbering is taken from the α-subunits of Kp1 structure 1QGU and Av1 structure 2MIN in the Brookhaven protein data bank.

Scheme 1: Model Structures Used for the DFT Calculations: (a) $x = 1$ or 2; (b) $x = 0$ or 1, $y = 0$ or 1; (c) $x = 0$ or 1, $y = 0$ or 1[a]

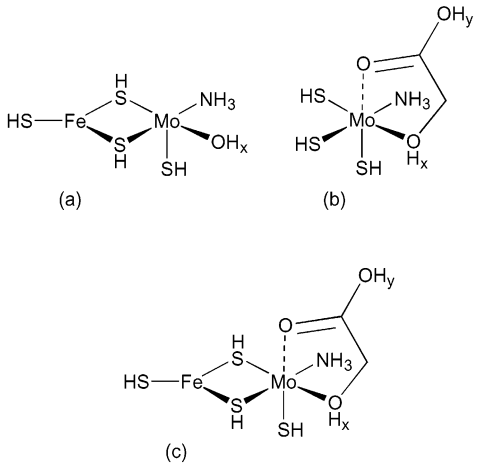

[a] Dashed bonds were absent in ring-opened models.

coordinated N_2. Analysis of the Av1 structure gave very similar results. In summary, five of the six central Fe atoms are very poorly discriminated in terms of their ability both to bind and to protonate N_2.

DFT Calculations. The subsections of the FeMoco used in the DFT studies are shown in Scheme 1, and the output from the calculations is summarized in Figures 2 and 3. All spin state permutations considered possible (up to four states) were investigated for each of the structures shown in Figure 3. For all of the ground state structures, the calculated spin density on Fe was relatively invariant at 3.1−3.7, regardless of whether the structure was formally Fe^{II} or Fe^{III}. The spin on Mo was more variable, ranging from ∼0 for structure **19** (formally Mo^{VI}) to 2.9 for **13** (formally Mo^{III}). Generally, antiferromagnetic coupling between Fe and Mo was preferred, except those for **13** and **22**, for which ferromagnetic coupling was marginally more stable. The optimized DFT geometries generally overestimated the terminal and bridging M−S bond lengths by 3−6% and 10−13%, respectively, compared to the crystal structure values; similar trends have been found for the same DFT method applied to structurally related simple Fe complexes, whereas other bond lengths were more accurately reproduced (*34*). Concerning the Mo−N and Mo−O distances, detailed comparison with experiment is hampered by significant disagreements in the available data. For example, a Mo−N (His) distance of 2.15 Å was found in the Av1 crystal structure (*11*), but the equivalent distance in the higher resolution Kp1 structure was 2.48 Å (*13*). Similarly, the average Mo−O distance was 2.04 Å for Av1 but 2.32 Å for Kp1, while EXAFS studies gave an overall Mo−O/N distance of ca. 2.2 Å (*35*). In the present DFT study, the calculated Mo−N and Mo−O distances in **1** were 2.25 and 1.93 Å respectively.

The first crucial consideration for involvement of molybdenum in catalysis concerns the energetic feasibility of opening the homocitrate ring. To address this question, DFT calculations were carried out on model sites containing a glycolate ligand as a simple homocitrate analogue, Scheme 1b,c. By the use of both mononuclear and dinuclear models, the effects of different levels of protonation of the oxygens and different Mo oxidation states could be compared. The optimized structures and their relative energies are given in

Figure 2. In this and subsequent figures, the energy changes for the reactions indicated or the relative energies of the individual structures as appropriate (in kcal mol^{-1}) are given in parentheses, with one structure at each redox level arbitrarily assigned as the reference state. The first important result from these calculations is that the ease of chelate ring opening is determined primarily by the state of protonation of the carboxylate group. Thus, addition of an H atom to the noncoordinated carboxylate oxygen atom reduces the cost of chelate ring opening from +37 to +8 kcal mol^{-1}. This situation is analogous to organic substitution reactions, where protonation of carboxylate invariably makes it a better leaving group. Other factors such as the oxidation state of Mo and protonation of the alkoxide oxygen have smaller effects. A further point of interest is that all of the ring-opened structures show a hydrogen bond between the carboxylic oxygen and the NH_3 ligand, which appears to be responsible for the existence of structures **2**, **4**, **6**, and **8** as local minima. Although this hydrogen bond is serendipitous, in the sense that the NH_3 group is present as a model for the imidazole ligand to Mo, it highlights the likely role of hydrogen bonds in facilitating homocitrate ring opening. We have previously postulated a stabilizing hydrogen bond between the homocitrate $CH_2CH_2CO_2^-$ arm and a conserved lysine in the ring-opened conformation, along with a weaker, Mo-activating hydrogen bond to the coordinated histidine (*14*). The pool of water molecules around the homocitrate might also make a contribution in this regard. Finally, ring opening followed by coordination of N_2, as in conversion of **7** to **9**, is exothermic overall, in this case by −10 kcal mol^{-1}. Hence, the hypothesis of transient homocitrate ring opening allowing coordination of N_2 at Mo is entirely consistent with the present DFT calculations.

The point charges on the carboxylic and alcoholic protons in **7**−**9** are very similar (0.40−0.42 and 0.39−0.43, respectively), suggesting that these groups might have similar pK_a's. There are good precedents for the protonation of both types of group in model complexes. For example, molybdenum complexes containing alcohol ligands (Mo−OHR) are well-known. Indeed, dialcohol ligands can display simultaneous Mo−OR and Mo−OHR coordination, as, for example, in the methoxide-bridged dimeric complex [{MoO_2($OCMe_2$-CMe_2OH)(OMe)}$_2$] (*36*). In the crystal structure of the complex $[MoO_2(Hmal)_2]^{2-}$ (H_3mal = malic acid, HO_2CCH_2-$CH(OH)CO_2H$), the alcohol group is coordinated to Mo and deprotonated, and the remaining acidic proton is located approximately midway between the coordinated and non-coordinated carboxylate groups (*37*), emphasizing the importance of hydrogen bonding in the protonation state of coordinated carboxylate. In principle, the Mo−O bond lengths could be used to assess the protonation state of the homocitrate in nitrogenase, since the calculated geometries show significant increases for both types of Mo−O bond on protonation, as also noted previously (*16*). However, in view of the disagreements between the available crystal structures and EXAFS data discussed above, this cannot be done with confidence at present. One feature which is clearly supported by the nitrogenase crystal structures is that protonation of homocitrate may be facilitated by water. Thus, although the FeMoco is completely buried within the protein, there is a pocket of ca. 20 water molecules within about 5 Å of the homocitrate. This "water pool" (*2*) shows extensive hydrogen bonding with the homocitrate oxygens and moreover is in contact with the exterior of the protein via a water-filled channel (*28*). Therefore, there should be a ready supply of protons to the homocitrate end of the FeMoco during catalysis. The water pool also gives space for ring-opening of homocitrate and coordination of N_2 with minimal perturbation of the surrounding protein (*14*).

Given the availability of a coordination site on Mo upon reduction, the character of N_2 binding at both the trigonal Fe sites and the Mo site of the FeMoco needs to be considered. The results of DFT calculations on the various possibilities for N_2 binding and initial protonation using the dinuclear model **10**, Scheme 1a, are shown in Figure 3. The intrinsic N_2 BE's at the Fe^{II} and Mo^{III} sites are −8 and −13 kcal mol^{-1}, respectively. Clearly, weak binding of N_2 at both the Fe and Mo sites is predicted, with the Mo site moderately preferred over Fe. The N_2 BE for the Mo site is the same as that calculated for the Mo^{III} amide complex [$Mo(N_2)(NH_2)_3$] (*15*). Experimentally, N_2 is weakly bound at [Mo{N(R)Ar}$_3$] sites [R = $C(CD_3)_2CH_3$, Ar = 3,5-$C_6H_3Me_2$], and the N_2 complex cannot be isolated from solution (*38*). Interestingly, the N_2 ligand is nevertheless found to be strongly activated, in this case with respect to cleavage to the corresponding nitride.

A more dramatic difference between the Fe- and Mo-bound N_2 ligands is found in their ease of reduction. It is well-known that the first N_2 reduction step, to the diazenido-(1−) (NNH) ligand, is energetically the most difficult. In the present model, the Mo-bound diazenido intermediate **14** was found to be significantly more stable than its Fe-bound counterpart **13**, with an energy difference between the two isomers of 17 kcal mol^{-1}. Most interestingly, when the MoNNH species was input into the geometry optimization in a terminally bound mode, similar to the N_2 complex **12**, it spontaneously adopted the bridging mode shown in **14**. The net stabilization gained by bridging to the Fe atom is approximately 5 kcal mol^{-1}. The NNR-$\mu-\eta^2$ bridging geometry predicted in this study has been observed experimentally in a number of dinuclear complexes, and the calculated N═N bond length of 1.27 Å for **14** agrees very well with the experimentally observed range of 1.20−1.29 Å (*39*). A particularly relevant example in the current context is the dinuclear complex [$Mo_2(C_5H_5)_2(\mu$-$SMe)_3$(NNMe-$\mu-\eta^2$)], which has an N═N bond length of 1.20 Å (*40*). Like its phenyl analogue, this NNR-$\mu-\eta^2$ complex was found to be in equilibrium with its NNR-$\mu-\eta^1$ isomer (*41*). However, in the present calculations, the NNH-$\mu-\eta^1$ isomer **15** was found to be 15 kcal mol^{-1} less stable than **14** and can be excluded.

Addition of a further H^+/e^- couple to **14** gives the N_2H_2 isomers **16**−**18**. The bridging (**16**) and linear (**17**) hydrazido-(2−) structures are both local minima and essentially isoenergetic, while the bridging diazene isomer **18** is only a little higher in energy, and cleavage of the diazenido(2−) ligand to give **19** can be ruled out at this redox level. Experimentally characterized (NNR_2-η^2) complexes comparable to **16** are very rare compared to their well-known η^1 isomers. Nevertheless, Glassman et al. (*42*) have characterized complexes [(C_5Me_5)WMe_3(NNHR-η^2)] (R = H or Me) in solution; these isomerize readily to the η^1 isomers, apparently to relieve steric congestion. Regarding precedents for structure **18**, several bridging diazene complexes have

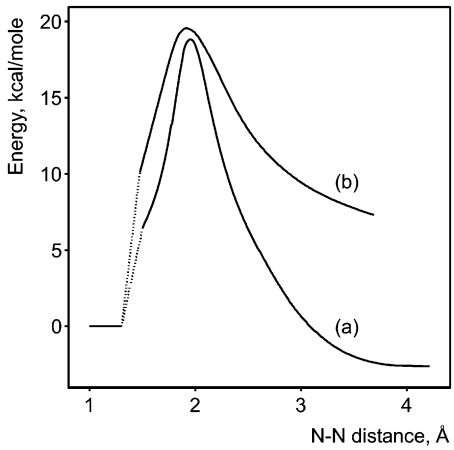

FIGURE 4: Plots of energy vs N−N distance for N−N bond cleavage. Curve a, transformation of **21** into **23**; the horizontal line represents the energy of structure **21**, taken as the reference state. The spin state of all three species is $S = 2$. The dotted line represents the transformation of the linear NNH_2 species **21** into the bridging form **20**. Curve b, transformation of **24** into **26**; here, the horizontal line represents **24**, $S = 1$, taken as the reference state, while the species described by the curve have spin $S = {}^5/_2$. The dotted line represents the promotion of **24** from the $S = 1$ to the $S = {}^5/_2$ spin state.

been described; perhaps the most relevant here are [{Fe("S_4")$(PPh_3)_2$}$_2$(NHNH-μ-η^2)] ["S_4" = $(CH_2SC_6H_4S^-)_2$] (*43*) and [$(C_5H_5)Mo_2(\mu$-SMe$)_3$(NHNPh-μ-η^2)] (*41*), both of which have been fully characterized.

The metal oxidation states in **17** are Fe^{II} and Mo^{V}. It has been assumed in this study for the reasons given in the discussion of the Lowe−Thorneley state E_5 (see below) that the next H^+/e^- couple is added to the FeMoco core rather than the N_2H_2 ligand. This was modeled by replacing the OH ligand to Mo with OH_2, giving isomers **20**−**22**. The order of stabilities in this redox manifold is different from that of the previous one; the diazene species **22** is now more stable than the hydrazido(2−) species **20** and **21**. Cleavage of the N−N bond to give **23** is also now energetically allowed. Once formed, the NH_2 ligand in **23** would rapidly protonate to give ammonia (cf. structure **27**), driving the reaction to completion. The energetics of cleavage of the N−N bond under these conditions were studied, with the results shown in Figure 4. The first step in the cleavage pathway is the transformation of the linear hydrazido(2−) species **21** into its bridged form **20**, shown by the dotted part of curve (a). The energy barrier for conversion of **21** to **23** was then estimated by carrying out a series of calculations in which the N−N distance was constrained to a series of values between those found in **20** and **23** (1.50 to 4.21 Å, respectively). The energy maximum occurred at an N−N distance of 1.95 Å and an energy of +12 kcal mol^{-1} relative to **20** (+19 kcal mol^{-1} relative to **21**), suggesting that cleavage of the N−N bond in **21** is both thermodynamically and kinetically feasible. However, the rate of cleavage at this redox level could be attenuated by competition from the bridging diazene isomer **22**, which would not itself undergo N−N bond cleavage. If so, further substrate-based reduction would then be required, giving the ($NHNH_2$-μ-η^2) species **24**. Cleavage of the N−N bond at this stage to give **26** was also investigated (Figure 4). This time, the first step is promotion of the $S = {}^1/_2$ ground state (formally Fe^{II}, Mo^{III}; calculated spins +3.6 and −2.9, respectively) to an $S = {}^5/_2$ excited state (calculated spins Fe +3.6, Mo +1.1), shown by the dotted line in curve b. The curve for N−N bond cleavage was then calculated as before, giving an overall maximum of +20 kcal mol^{-1} at an N−N distance of 1.92 Å. The initial cleavage product **26** rearranges easily to structure **27**; indeed, the calculation of curve b required an extra geometrical restraint in order to prevent spontaneous rearrangement to **27** for N−N distances above 2.4 Å. It is possible that the value of the energy required to promote the spin state of **24** prior to cleavage may be overestimated due to the limited size of the FeMoco model used in the present calculations; if so, the true energy barrier for cleavage of the N−N bond at this redox level may be lower than indicated by these results.

The alternative structure to **24**, namely, the NNH_3 isomer **25**, is interesting in that calculations on the $S = {}^3/_2$ spin state resulted in spontaneous cleavage of the N−N bond to give a molybdenum nitride plus ammonia, without any direct involvement of the Fe site. For this reason, **25** is the only structure in the figures which is not a local minimum; it was produced by constraining the N−N bond to 1.56 Å, the mean value obtained from the $S = {}^5/_2$ and ${}^7/_2$ spin states, which did not show N−N cleavage. Spontaneous cleavage of the NNH_3 ligand was also observed by Dance in his DFT studies (*22*); in this case, the reaction was modeled on an Fe_4 "face" of the FeMoco. However, in the current work, the initial formation of **25** can be ruled out as this species is much higher in energy than **24**. It is worth noting here that DFT calculations using the same method as the present studies predicted $[MoCl(NNH_3)(PH_3)_4]^{2+}$ to be 11 kcal mol^{-1} more stable than $[MoCl(NHNH_2)(PH_3)_4]^{2+}$ (*44*), in agreement with the experimental isolation of $[MoCl(NNH_3)(PMe_3)_4]Cl_2$ (*45*).

DISCUSSION

Initial Binding of Dinitrogen at the FeMoco. The ability of the FeMoco to bind small molecules such as N_2, H_2, and CO depends on a number of factors. As well as the constraints imposed by the protein environment, there are electronic considerations. The first of these is the overall redox level of the FeMoco core cluster. The DFT calculations of Rod and Nørskov (*24*) suggest that this is not decisive in determining the strength of binding at single trigonal Fe sites provided that the overall charge on the cluster is constant. However, these authors did find a significant variation in the CO and N_2 BE's when the charge on the cluster was varied; for example, binding of CO was significantly stronger when a negative charge was placed on the cluster, and especially so when the NH_4^+ counterion was able to interact with the bound CO. In addition to reduction steps of this type, in which e^- is formally added to the FeMoco core and H^+ to a nearby amino acid, it is possible to add both the electron and the proton to the FeMoco cluster itself. This has been demonstrated for isolated FeMoco in NMF solution, where reduction is accompanied by two successive protonation equilibria (*46*). Calculations indicate that the preferred sites for H atom addition are the three central sulfurs of the FeMoco (*24*).

The predicted weak binding of N_2 at both the Fe and Mo sites of the FeMoco raises an important problem, since the solubility of N_2 in water is only ~0.7 mM. To effectively capture N_2 from solution, nitrogenase must build up the local

concentration of N_2 at the active site. A similar problem pertains in hydrogenases, where H_2 must be captured from solution. Like nitrogenase, the active site of Ni−Fe hydrogenase from *Desulfovibrio fructosovorans* is buried in the protein matrix. However, the hydrogenase active site is connected to the protein exterior by a network of hydrophobic cavities. Treatment of the protein with xenon allowed the observation of approximately ten Xe atoms within the structure, located within these cavities (*47*), and it was concluded that the hydrophobic pockets serve to concentrate H_2 in the vicinity of the active site. However, a similar analysis on nitrogenase (*48*) located only four Xe binding sites per $\alpha\beta$-dimer, and of these, only two were buried within the protein. This suggests that although nitrogenase shares a common problem with hydrogenase in terms of accumulation of substrate concentration at the active site, it utilizes a different solution. One possible answer is suggested by the analysis of N_2 binding at the Fe sites of FeMoco, given in Table 1. Five of the six central Fe atoms are available for weak binding of N_2. Since the FeMoco is wholly enclosed by the protein, this suggests a mechanism whereby N_2 or other small molecules might be concentrated at the active site; the FeMoco itself attracts N_2 by transient, nonspecific binding to multiple Fe sites during the early stages of catalysis (i.e., at levels in the Lowe−Thorneley scheme which do not detectably bind N_2). There are two important points which follow from this hypothesis. First, since there is a limit to the available volume around the FeMoco (in that N_2 or other species must approach the cofactor by displacing water molecules from its vicinity), there must be a strict limit to the number of hydrophobic molecules (N_2, H_2, CO etc.) which can accumulate in the FeMoco pocket. This may give rise to subtle competitive effects. Second, since CO usually binds to metal sites in an analogous, but stronger, fashion to N_2, nitrogenase should exhibit multiple CO binding modes. This is indeed the case. Thus, in studies on isolated FeMoco, between two and four CO bands were always observed when the FeMoco was reduced under a CO atmosphere (*49*). Similarly, stopped-flow infrared measurements on nitrogenase under turnover conditions showed four CO bands for a CO concentration of 0.5 mM under turnover conditions (*50*). The use of a lower concentration of CO (60 μM) did give a single CO band; however, the signal-to-noise ratio of this spectrum was ~9, and hence bands of 10-fold lower intensity would not be observed. In terms of energy, a 10-fold ratio in equilibrium concentrations between two different CO-bound species would require an energy difference of only 1.4 kcal mol^{-1}. CO binding to the FeMoco has also been studied by ENDOR spectroscopy (*51*). In these studies, a single CO-bound form of FeMoco was observed under a partial pressure of 0.08 Atm of CO, while at 0.5 Atm of CO, a second CO was found to bind to the same FeMoco moiety (note that molecular modeling readily shows the impossibility of binding more than one CO at a single trigonal Fe atom of the FeMoco). These spectroscopic results are fully consistent with the concept of binding of CO (and, by extension, N_2) to multiple Fe sites on the FeMoco, with small energy differences between the different binding modes; hence, observation of a single CO-bound species requires very low solution concentrations of CO. Another interesting observation in this context relates to a mutant Av nitrogenase in which α-Arg^{277} was substituted by His (*52*). Experiments on this mutant's inhibition of C_2H_2 reduction by low concentrations of CO were interpreted in terms of two independent sites for C_2H_2 reduction, inhibited by CO binding at a third site.[3]

Homocitrate Ring Opening. Although poorly discriminated binding of N_2 to multiple Fe sites of the FeMoco may serve a useful purpose in terms of raising the local concentration of N_2, it seems most unlikely that the reduction of the biological substrate N_2 would proceed indiscriminately on this basis. However, opening of the homocitrate ring produces a new, unique site; in the case of Mo nitrogenase, this is the Mo atom. The DFT calculations presented here indicate that homocitrate ring opening is energetically feasible, and that N_2 binds preferentially at Mo once this site is available.

Experimentally, the activities of nitrogenase preparations display an exquisite sensitivity to chemical modifications of the homocitrate ligand, especially with respect to N_2 reduction (*25*−*27*). Replacement of homocitrate by citrate in an in vitro synthesis of FeMoco diminished the enzyme's N_2-reducing activity to 7−17% of that observed with homocitrate (*26*, *27*). We have interpreted this result in terms of the formation of a hydrogen bond between the $CH_2CH_2CO_2^-$ arm of homocitrate and the imidazole ring hydrogen of α-His^{442} (Av1) upon opening of the homocitrate chelate ring (*14*). Citrate is incapable of an analogous interaction.[4]

[3] It should be noted that CO appears to be a noncompetitive inhibitor of both N_2 and acetylene reduction, as shown by the lack of a common intercept in the respective Lineweaver−Burk plots (*53*), although the K_i's reported appear to be close to the concentration of the MoFe−protein. If the inhibition is indeed noncompetitive, this can be accommodated within the model described in this paper as follows. Under low CO conditions, reduction of N_2 at the Mo−Fe7 face of the FeMoco will be inhibited by binding of the electron-withdrawing CO ligand at one of the other Fe sites. In principle, a higher pressure of N_2 would relieve this inhibition via displacement of the CO by a second N_2 ligand. However, CO binding to a given metal centre is invariably much stronger than N_2 binding at the same site. According to Rod and Nørskov's calculations, the CO binding energy at a single trigonal Fe site of the FeMoco is ~24 kcal mol^{-1} higher than that of N_2 (*24*). This means that a pN_2 in the order of thousands of Atmospheres would be required to detect competitive inhibition (manifested by deviations in linearity towards a common intercept in the Lineweaver−Burk plot) under typical experimental conditions. A similar argument can be made for inhibition of acetylene reduction by CO.

[4] Our hypothesis requires that the NH group of the histidine imidazole ring which acts as a ligand to Mo remains protonated throughout the catalytic cycle. It has recently been suggested from DFT calculations that the imidazole ring might be deprotonated in the enzyme's resting state (*16*). This followed from a comparison of the calculated Mo−N bond lengths for neutral and deprotonated methylimidazole ligands (2.31 and 2.16 Å, respectively) with the Mo−N bond length of 2.15 Å obtained from the Av1 crystal structure (*11*). However, several pieces of experimental data are relevant here. First, the higher resolution Kp1 structure returned a much longer Mo−N distance, of 2.48 Å (*13*). Second, the X-ray crystal structures of imidazole and imidazolate complexes show that in general, the M−N bond length does vary a little with the state of protonation of the imidazole ligand, but is also linked to the spin state of the metal (*54*−*56*). Given the pH's used to obtain the Kp and Av crystal structures (8.0 and 8.5, respectively), in order for the Mo−His imidazole to be 90% deprotonated, its pK_a would have to be ≤7.5. Measurements on imidazole coordinated to a range of metal centres gave significantly higher pK_a values, of 8.9−11.4 (*57*). Finally, the normal pK_a of a carboxylate group is ~4.8. Given the pK_a range observed above for coordinated imidazole, it seems unlikely that a single proton would add to carboxylate rather than imidazolate. However, if both the homocitrate and imidazole groups are deprotonated in the protein, it is very difficult to conceive of any significant interactions between these two groups, and the $NifV^-$ experimental data would be inexplicable.

A particularly intriguing set of experiments was conducted on fluorohomocitrate isomers (*25*). In these studies, in vitro synthesis was used to incorporate modified forms of FeMoco, containing fluorohomocitrate isomers, into the MoFe protein. Whereas *erythro*-fluorohomocitrate retained 25−30% of the N_2 reduction activity of homocitrate itself, *threo*-fluorohomocitrate showed virtually no N_2 reduction at all. These isomers have been examined by molecular modeling in the present study. First, on modeling the two isomers into the Kp crystal structure, neither fluorine atom has any potential for forming new hydrogen bonds with the surrounding protein. The *erythro*-fluorine atom projects into the homocitrate water pool and, consequently, has essentially no effect on the protein structure. The *threo*-fluorine has a rather close contact with S3B of the cluster core; this can be relieved by adjustment of the torsion angles in the $CHFCO_2^-$ arm, but this perturbs the hydrogen bond between the $CHFCO_2^-$ arm of the fluorohomocitrate and the NH_2 group of α-Gln^{190} (α-Gln^{191} in Av1). This could impact on the enzyme's activity, since this hydrogen bond is implicated in electron transfer from the P-cluster (*14*). In the homocitrate ring-opened conformations, this steric congestion around the *threo*-fluorine atom becomes even more acute due to the rotation of the homocitrate CO_2^- arm through ∼90° following dechelation, whereas once again the *erythro*-fluorine has little effect on its surroundings.

Reduction of Dinitrogen. A more crucial distinction between the Mo and Fe sites of the FeMoco than the difference in N_2 BE's noted above is the difference in stabilities of the first reduced N_2 intermediates. Thus, the MoNNH species **14** is 17 kcal mol^{-1} more stable than the FeNNH species **13**. Given that addition of the first H atom to N_2 is thermodynamically the most difficult step, this energy difference is potentially very important. It arises in part from the distinctive topology of the FeMoco core cluster. Whereas the tetrahedral geometry of the Fe atoms in a cluster of the $[Fe_3MS_4]$-type precludes their direct involvement in chemistry occurring at the heterometal, the low coordination number of the Fe atoms in FeMoco, together with the inherent flexibility of the cluster as suggested by EPR analysis (*58*) and by DFT calculations (*24*), allows the Fe atom adjacent to the Mo atom's free coordination site (Fe7 in Figure 1) to participate directly in the chemistry occurring at Mo, via the formation of bridging N_2 intermediates such as **14**. This appears to be a key feature of the chemistry of FeMoco, not just for the initial protonated N_2 species but also for more reduced states in which it facilitates cleavage of the N−N bond (see below).

Extensive chemical studies have revealed a number of possible isomers for reduced N_2H_x species when $x = 2$ or 3; these have been compared, as shown in Figure 3. It seems likely from the results obtained that some nitrogenase redox states consist of equilibria between different partially reduced N_2 intermediates, most notably hydrazido(2−) and diazene isomers. During catalysis, nitrogenase must carry out two fundamental chemical reactions: N−H bond formation and N−N bond cleavage. The order of these reactions is not known from experiment, although the present and previous (*24*) DFT studies rule out an initial scission of the N−N bond, as occurs in the Haber process. Unfortunately, the exact nature of the N−N bond cleavage step is also unknown in many of the available chemical models. The results from this study suggest that for nitrogenase it can occur following the addition of two or three protons to the N_2 ligand and is facilitated by bridging of the reduced N_2 species between Mo and Fe across the face of the $MoFe_3S_3$ sub-cube of the FeMoco. As noted above, this appears to be a critical feature of the FeMoco's very distinctive structure. If there is not an efficient pathway for N−N bond cleavage, some of the product will be diverted to hydrazine rather than ammonia; this is observed for many chemical model systems as well as for vanadium nitrogenase (*1*).

Assignment of States within the Lowe−Thorneley Scheme. The course of N_2 reduction described above can be used to deduce an atomic mechanism for nitrogenase based upon the MoFe protein cycle of the Lowe−Thorneley scheme (*18*). The overall mechanism is shown diagrammatically in Scheme 2. In the following discussion, it is assumed that each electron added to the MoFe protein is associated with the movement of a proton to a specific location. However, the proton does not necessarily become attached to the substrate or the FeMoco core cluster; it may rather be added to a protein residue or to homocitrate. Such nonlocated protons are designated with circles in Scheme 2. Each state may also involve proton equilibria between two or more individual species. Hence the designation of hydrogen atoms in individual states E_1, E_2, etc. has been omitted for simplicity.

Spectroscopic and theoretical studies have been used to assign the resting state FeMoco cluster core as $[MoFe_7S_9]^+$ (*4*, *6*) or $[MoFe_7S_9]^{3+}$ (*5*). It will be assumed here that the former assignment corresponds to E_0 in the Lowe−Thorneley scheme. The first reduction will then give E_1 as $[MoFe_7S_9]^0$. A distinctive feature of state E_1 compared to E_2−E_4 is that it does not give a measurable release of H_2, either at pH 7.4 during turnover or on quenching (*17*). In an earlier analysis of the protonation characteristics of the FeMoco, loss of H_2 from reduced FeMoco states was interpreted in terms of the migration of H atoms from their initial sites of addition at the central S atoms of the FeMoco onto neighboring Fe atoms, with subsequent hydrolysis to H_2 (*28*). Since E_1 does not give H_2, it may be deduced that the proton associated with the first electron is not added to the FeMoco core but, rather, to an organic residue in the vicinity of the cluster; state E_1 can then be written as in Scheme 2. Rod and Nørskov found from their DFT studies that binding of N_2 and CO at the trigonal Fe atoms of the FeMoco was significantly affected by the overall charge on the cluster (*24*). Hence, in the present model state E_1 should have a higher affinity for N_2 and CO than E_0; this would explain why binding of CO is only observed under turnover conditions (*50*) and also allow N_2 to begin accumulating in the FeMoco pocket at state E_1 by weak, nonspecific interactions with the Fe atoms.[5]

The second reduction gives state E_2, which does release H_2. Following the reasoning outlined above, this state therefore possesses a hydrogenated FeMoco core, i.e., $[MoFe_7S_8(SH)]^0$. Previous analysis (*28*) indicated that protonation of the core cluster is kinetically controlled and that S2B receives

[5] Another possibility, suggested by very recent DFT calculations (*59*), is that the first proton is inserted into the centre of the FeMoco core cluster. This would be consistent with the present model, provided that the resulting species is not hydridic enough to give H_2 on acid quench.

Scheme 2: Proposed Model for Nitrogenase Catalysis[a]

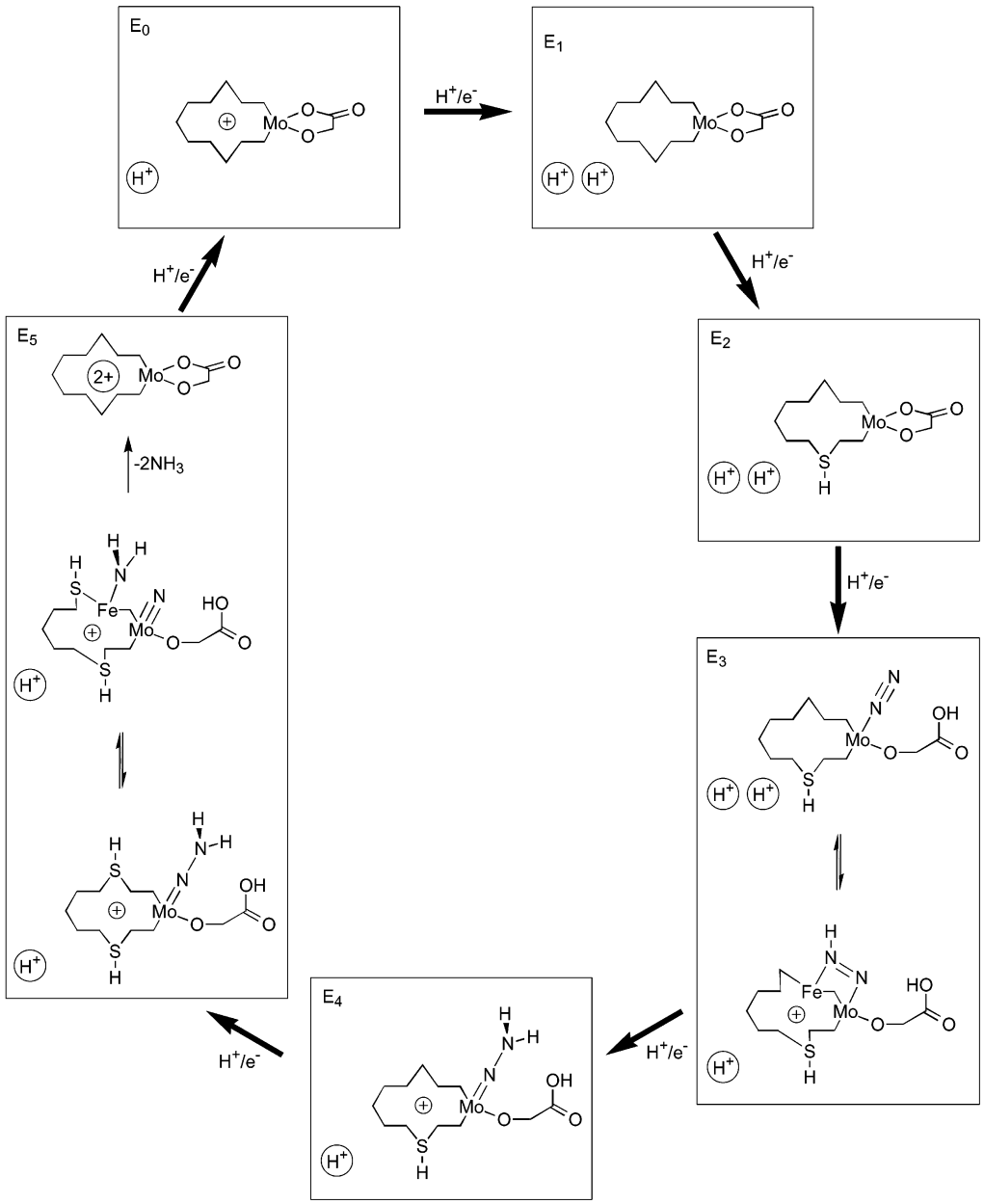

[a] For clarity, the FeMoco core cluster is shown schematically, and only the chelate ring of the homocitrate ligand has been included. The designations E_0, E_1 etc. refer to the Lowe−Thorneley scheme [ref *17*]. Each of the bold arrows represents the transfer of a single e^- from the Fe protein to the MoFe protein. Circled H^+ represent nonlocated protons associated with the protein or homocitrate.

the first proton. Under slow turnover conditions, this hydrogen atom will eventually be lost as H_2, returning the system to state E_0.

The distinctive attribute of state E_3 is that it is the first state to bind N_2 in the Lowe−Thorneley scheme. In the present model, this is explained by opening of the homocitrate ring on reduction to state E_3. The substrate N_2, which up to this point has been loosely associated with the FeMoco due to weak binding at the Fe atoms, can now migrate to Mo. Binding of N_2 at Mo is still reversible, but sufficiently strong to be detectable experimentally. Given the sensitivity of homocitrate ring opening to the protonation state of the carboxylate group, as demonstrated by the DFT calculations, the E_3 proton is probably added to the homocitrate CO_2^- arm. Binding of N_2 at this redox level may well be stabilized by reversible transfer of a proton from the surrounding protein to N_2 to give the NNH intermediate, as shown in Scheme 2.

MNNH complexes are generally unstable with respect to deprotonation to the N_2 complex or further reduction; hence, the next state, E_4, can be assigned to further reduction of substrate to give an NNH_2 (or possibly an HNNH) intermediate. It was shown that E_4 is responsible for the release of hydrazine from nitrogenase upon quenching the functioning enzyme at pH 0 or 14 (*18*); although this was taken to imply an NNH_2 intermediate, an HNNH species could also give hydrazine. Cleavage of the N−N bond to give an iron amide and molybdenum nitride at this redox level is unfavorable by more than 20 kcal mol^{-1}, apparently a consequence of the redox level of the Mo atom, which would need to reach Mo^{VI} in the nitride.

This situation changes at the next state, E_5. Previous studies of proton-transfer pathways through the protein indicated that two of the three central S atoms of the FeMoco become protonated during catalysis (*28*). By using this second proton channel to further reduce the core cluster via protonation of S5, cleavage of the N−N bond now becomes energetically feasible, resulting in a Mo^V nitride. Although the N−N bond cleavage step is approximately thermoneutral, the $FeNH_2$ species, once formed, should readily accept a further proton to give $FeNH_3$, so driving the reaction to completion. It was suggested (*28*) that protons added to S2B and S5 of the FeMoco during turnover might subsequently be discharged back to solvent, allowing for rapid proton rearrangements of this type. Note that the initial E_5 state can readily be reformulated as containing a bridging $NHNH_2$ ligand, by transfer of the nonlocated proton to the substrate. This would allow cleavage to proceed via the pathway shown in Figure 4b rather than 4a; these two possibilities are not mutually exclusive, and appear to have very similar energy profiles (Figure 4).

Further rapid proton rearrangements within the E_5 redox level would allow reduction of the nitride at the expense of the FeMoco core, giving the second molecule of ammonia without any further requirement for electron transfer from the Fe protein to the MoFe protein. The final state of the FeMoco in the E_5 level would then be oxidized by one electron compared to the E_0 level; there is extensive experimental evidence for such a state (*3*). Alternatively, this electron could be supplied by the P-cluster, which is also capable of supporting different redox levels (*3,13*). The present DFT calculations indicate that the molybdenum nitride bond in FeMoco is relatively weak compared to, say, $[MoN(NR_2)_3]$-type complexes (*15*). For example, the addition of an H atom to the nitride ligand in Figure 3, structure **23** to give **26** is calculated to be 30 kcal mol^{-1} more favorable than the addition of an H atom to the N_2 ligand in **12** to give **14**. This would be an important property of nitrogenase, since it metal nitrides are often unreactive "sink states" and therefore poor catalytic intermediates.

The proposed mechanism for N_2 reduction by nitrogenase shown in Scheme 2 is in good agreement with the Chatt cycle for N_2 fixation, reviewed in reference (*10*). The main differences stem from the fact that the Chatt cycle was worked out primarily on mononuclear complexes; hence, the potential significance of bridging N_2H_X intermediates was not so readily apparent as in more recent work on binuclear complexes (*40*, *41*). Also, the development of the Chatt cycle required the use of highly electron-rich metal centers to facilitate the isolation of some species. In the enzyme, the equivalent states, for example, the initial N_2 complex itself, would need to be much more labile in order to achieve efficient catalysis in vivo; hence, the FeMoco metal centers are less electron-rich than those in the model complexes.

In the Lowe−Thorneley scheme, two more steps, E_6 and E_7, are included in the catalytic cycle. This follows from the hypothesis that OHE is a necessary feature of the nitrogenase mechanism. None of the steps in the mechanism described above require OHE; although it might be possible to modify the present model to include such a requirement, it does not seem to follow naturally from the chemistry. Issues related to H_2/N_2 competition and the HD formation reaction will be dealt with more fully in the following paper. It is, however, worth noting here that there is no direct experimental evidence for states E_6 and E_7.

ACKNOWLEDGMENT

I thank C. J. Pickett, D. J. Lowe, D. M. Lawson, and S. J. George (John Innes Centre), R. A. Henderson (University of Newcastle), K. Fisher (Virginia Tech), and J. Talarmin (Université de Bretagne Occidentale) for helpful discussions.

NOTE ADDED IN PROOF

Very recently, the X-ray crystal structure of nitrogenase has been revised to include an additional atom, most likely N, in the center of the FeMoco core cluster (*60*). This modification would be expected to deactivate the central Fe atoms with respect to dinitrogen binding and reduction, since (1) they can no longer be viewed as three-coordinate and (2) a trans-nitride interaction is likely to be deactivating with respect to formation of partially reduced dinitrogen species on Fe. The properties of the Mo atom should be less perturbed, since it is more remote from the new atom. Hence, this new observation probably strengthens the case for direct participation of the Mo site in nitrogen fixation.

REFERENCES

1. Eady, R. R. (1996) Structure−function relationships of alternative nitrogenases, *Chem. Rev. 96*, 3013−3030.
2. Howard, J. B., and Rees, D. C. (1996) Structural basis of biological nitrogen fixation, *Chem. Rev. 96*, 2965−2982.
3. Burgess, B. K., and Lowe, D. J. (1996) Mechanism of molybdenum nitrogenase, *Chem. Rev. 96*, 2983−3011.
4. Lee, H.-I., Hales, B. J., and Hoffman, B. M. (1997) Metal-ion valencies of the FeMo cofactor in CO-inhibited and resting state nitrogenase by ^{57}Fe Q-band ENDOR, *J. Am. Chem. Soc. 119*, 11395−11400.
5. Yoo, S. J., Angove, H. C., Papaefthymiou, V., Burgess, B. K., and Münck, E. (2000) Mössbauer study of the MoFe protein of nitrogenase from *Azotobacter vinelandii* using selective ^{57}Fe enrichment of the M-centers, *J. Am. Chem. Soc. 122*, 4926−4936.
6. Lovell, T., Li, J., Liu, T., Case, D. A., and Noodleman, L. (2001) FeMo cofactor of nitrogenase: a density functional study of states M^N, M^{OX}, M^R, and M^I, *J. Am. Chem. Soc. 123*, 12392−12410.
7. Strop, P., Takahara, P. M., Chiu, H.-J., Angove, H. C., Burgess, B. K., and Rees, D. C. (2001) Crystal structure of the all-ferrous $[4Fe\text{-}4S]^0$ form of the nitrogenase iron protein from *Azotobacter vinelandii*, *Biochemistry 40*, 651−656.
8. Nyborg, A. C., Johnson, J. L., Gunn, A., and Watt, G. D. (2000) Evidence for a two-electron transfer using the all-ferrous Fe protein during nitrogenase catalysis, *J. Biol. Chem. 275*, 39307−39312.
9. Simpson, F. B., and Burris, R. H. (1984) A nitrogen pressure of 50 atm does not prevent evolution of hydrogen by nitrogenase, *Science 224*, 1095−1097.
10. Pickett, C. J. (1996) The Chatt cycle and the mechanism of enzymic reduction of molecular nitrogen, *J. Biol. Inorg. Chem. 1*, 601−606.
11. Peters, J. W., Stowell, M. H. B., Soltis, S. M., Finnegan, M. G., Johnson, M. K., and Rees, D. C. (1997) Redox-dependent structural changes in the nitrogenase P-cluster, *Biochemistry 36*, 1181−1187 and references therein.
12. Sørlie, M., Christiansen, J., Lemon, B. J., Peters, J. W., Dean, D. R., and Hales, B. J. (2001) Mechanistic features and structure of the nitrogenase α-Gln^{195} MoFe protein, *Biochemistry 40*, 1540−1549.
13. Mayer, S. M., Lawson, D. M., Gormal, C. A., Roe, S. M., and Smith, B. E. (1999) New insights into structure−function relationships in nitrogenase: a 1.6 Å resolution X-ray crystallographic study of *Klebsiella pneumoniae* MoFe-protein, *J. Mol. Biol. 292*, 871−891.
14. Grönberg, K. L. C., Gormal, C. A., Durrant, M. C., Smith, B. E., and Henderson, R. A. (1998) Why R-homocitrate is essential to the reactivity of FeMo-cofactor of nitrogenase: studies on $NifV^-$-extracted FeMo-cofactor, *J. Am. Chem. Soc. 120*, 10613−10621.

15. Durrant, M. C. (2001) A molybdenum-centred model for nitrogenase catalysis, *Inorg. Chem. Commun. 4*, 60−62.
16. Szilagyi, R. K., Musaev, D. G., and Morokuma, K. (2001) Theoretical studies of biological nitrogen fixation. I. Density functional modeling of the Mo-site of the FeMo-cofactor, *Inorg. Chem. 40*, 766−775.
17. Lowe, D. J., and Thorneley, R. N. F. (1984) The mechanism of *Klebsiella pneumoniae* nitrogenase action. Pre-steady-state kinetics of H_2 formation, *Biochem. J. 224*, 877−886.
18. Thorneley, R. N. F., and Lowe, D. J. (1984) The mechanism of *Klebsiella pneumoniae* nitrogenase action. Pre-steady-state kinetics of an enzyme-bound intermediate in N_2 reduction and of NH_3 formation, *Biochem. J. 224*, 887−894.
19. Lowe, D. J., and Thorneley, R. N. F. (1984) The mechanism of *Klebsiella pneumoniae* nitrogenase action. The determination of rate constants required for the simulation of the kinetics of N_2 reduction and H_2 evolution, *Biochem. J. 224*, 895−901.
20. Thorneley, R. N. F., and Lowe, D. J. (1984) The mechanism of *Klebsiella pneumoniae* nitrogenase action. Simulation of the dependences of H_2-evolution rate on component-protein concentration and ratio and sodium dithionite concentration, *Biochem. J. 224*, 903−909.
21. Peters, J. W., Fisher, K., and Dean, D. R. (1995) Nitrogenase structure and function: a biochemical-genetic perspective, *Annu. Rev. Microbiol. 49*, 335−366.
22. Dance, I. (1997) Calculated details of a mechanism for conversion of N_2 to NH_3 at the FeMo cluster of nitrogenase, *Chem. Commun.* 165−166.
23. Siegbahn, P. E. M., Westerberg, J., Svensson, M., and Crabtree, R. H. (1998) Nitrogen fixation by nitrogenases: a quantum chemical study, *J. Phys. Chem. B 102*, 1615−1623.
24. Rod, T. H., and Nørskov, J. K. (2000) Modeling the nitrogenase FeMo cofactor, *J. Am. Chem. Soc. 122*, 12751−12763.
25. Madden, M. S., Kindon, N. D., Ludden, P. W., and Shah, V. K. (1990) Diastereomer-dependent substrate reduction properties of a dinitrogenase containing 1-fluorohomocitrate in the iron−molybdenum cofactor, *Proc. Natl. Acad. Sci. U.S.A. 87*, 6517−6521.
26. Hoover, T. R., Imperial, J., Liang, J., Ludden, P. W., and Shah, V. K. (1988) Dinitrogenase with altered substrate specificity results from the use of homocitrate analogues for in vitro synthesis of the iron−molybdenum cofactor, *Biochemistry 27*, 3647−3652.
27. Imperial, J., Hoover, T. R., Madden, M. S., Ludden, P. W., and Shah, V. K. (1989) Substrate reduction properties of dinitrogenase activated in vitro are dependent upon the presence of homocitrate or its analogues during iron−molybdenum cofactor synthesis, *Biochemistry 28*, 7796−7799.
28. Durrant, M. C. (2001) Controlled protonation of iron−molybdenum cofactor by nitrogenase: a structural and theoretical analysis, *Biochem. J. 355*, 569−576.
29. *Chem-X*, version 1999.2 (1999) Oxford Molecular Ltd., Oxford.
30. Frisch, M. J., Trucks, G. W., Schlegel, H. B., Scuseria, G. E., Robb, M. A., Cheeseman, J. R., Zakrzewski, V. G., Montgomery, J. A., Jr., Stratmann, R. E., Burant, J. C., Dapprich, S., Millam, J. M., Daniels, A. D., Kudin, K. N., Strain, M. C., Farkas, O., Tomasi, J., Barone, V., Cossi, M., Cammi, R., Mennucci, B., Pomelli, C., Adamo, C., Clifford, S., Ochterski, J., Petersson, G. A., Ayala, P. Y., Cui, Q., Morokuma, K., Malick, D. K., Rabuck, A. D., Raghavachari, K., Foresman, J. B., Cioslowski, J., Ortiz, J. V., Stefanov, B. B., Liu, G., Liashenko, A., Piskorz, P., Komaromi, I., Gomperts, R., Martin, R. L., Fox, D. J., Keith, T., Al-Laham, M. A., Peng, C. Y., Nanayakkara, A., Gonzalez, C., Challacombe, M., Gill, P. M. W., Johnson, B. G., Chen, W., Wong, M. W., Andres, J. L., Head-Gordon, M., Replogle, E. S., and Pople, J. A. (1998) *Gaussian 98*, revision A.7, Gaussian, Inc., Pittsburgh, PA.
31. Berman, H. M., Westbrook, J., Feng, Z., Gilliland, G., Bhat, T. N., Weissig, H., Shindyalov, I. N., and Bourne, P. E. (2000) The Protein Data Bank, *Nucleic Acids Res. 28*, 235−242.
32. Sayle, R. (1993−1995) *RasMol*, version 2.4, Glaxo Research and Development, Greenford, U.K.
33. Hills, A., Hughes, D. L., Jimenez-Tenorio, M., Leigh, G. J., and Rowley, A. T. (1993) Bis[1,2-bis(dimethylphosphino)ethane]-dihydrogenhydridoiron(II) tetraphenylborate as a model for the function of nitrogenases, *J. Chem. Soc., Dalton Trans.* 3041−3049.
34. Davies, S. C., Durrant, M. C., Hughes, D. L., Richards, R. L., and Sanders, J. R. (2000) Iron, cobalt and vanadium complexes of the $N(CH_2CH_2S)_3^{3-}$ ligand with chloride, azide, cyanide and carbonyl co-ligands, *J. Chem. Soc., Dalton Trans.* 4694−4701.
35. Liu, H. I., Filipponi, A., Gavini, N., Burgess, B. K., Hedman, B., Di Cicco, A., Natoli, C. R., and Hodgson, K. O. (1994) EXAFS studies of FeMo-cofactor and MoFe protein: direct evidence for the long-range Mo−Fe−Fe interaction and cyanide binding to the Mo in FeMo-cofactor, *J. Am. Chem. Soc. 116*, 2418−2423.
36. Knobler, C., Penfold, B., Robinson, W. T., Wilkins, C. J., and Yon, S. H. (1980) Molybdenum(VI) complexes from diols and amino alcohols: the occurrence of MoO_2, Mo_2O_3, and Mo_2O_5 core structures, *J. Chem. Soc., Dalton Trans.* 248−252.
37. Knobler, C. B., Wilson, A. J., Hider, R. N., Jensen, I. W., Penfold, B. R., Robinson, W. T., and Wilkins, C. J. (1983) Molybdenum-(VI) complexes with malic acid: their inter-relationships, and the crystal structure of dicaesium bis[(*S*)-malato(2-)*cis*-dioxomolybdate(VI)-water (1/1), *J. Chem. Soc., Dalton Trans.* 1299−1303.
38. Cummins, C. C. (1998) Reductive cleavage and related reactions leading to molybdenum- element multiple bonds: new pathways offered by three-coordinate molybdenum(III), *Chem. Commun.* 1777−1786.
39. Yan, X., Batchelor, R. J., Einstein, F. W. B., and Sutton, D. (1996) Aryldiazenido complexes: synthesis of diiridium complexes with mono- and dibridging aryldiazenido ligands and X-ray structures of $[(\eta^5\text{-}C_5Me_5)IrI]_2(\mu\text{-}\eta^2\text{-}p\text{-}N_2C_6H_4OMe)(\mu\text{-}\eta^1\text{-}p\text{-}N_2C_6H_4OMe)$ and $[\{(\eta^5\text{-}C_5Me_5)Ir(CO)\}_2(\mu\text{-}\eta^2\text{-}p\text{-}N_2C_6H_4OMe)][BF_4]$, *Inorg. Chem. 35*, 7818−7828 and references therein.
40. Schollhammer, P., Didier, B., Le Grand, N., Pétillon, F. Y., Talarmin, J., Muir, K. W., and Teat, S. J. (2002) Transformations of hydrazines $RNHNH_2$ (R = Me, Ph) at a sulfur-rich bimetallic site: diazene-diazenido-isodiazene/hydrazido(2-) interconversions, *Eur. J. Inorg. Chem 3*, 658−663.
41. Schollhammer, P., Guénin, E., Pétillon, F. Y., Talarmin, J., Muir, K. W., and Yufit, D. S. (1998) η^1-η^2 rearrangement and protonation of phenyldiazo bridging ligands attached to the dimolybdenum system $\{Mo_2Cp_2(\mu\text{-}SMe)_3\}$, *Organometallics 17*, 1922−1924.
42. Glassman, T. E., Vale, M. G., and Schrock, R. R. (1992) Diamagnetic (pentamethylcyclopentadienyl)tungsten complexes containing unsubstituted, monomethyl, or 1,1-dimethyl hydrazine or hydrazido ligands, *J. Am. Chem. Soc. 114*, 8098−8109.
43. Sellmann, D., Friedrich, H., Knoch, F., and Moll, M. (1994) Transition metal complexes with sulfur ligands, C. Unexpectedly facile formation of diazene complexes and a new type of diastereoisomerism: $[\mu\text{-}N_2H_2\{Fe(PPr_3)(\text{'}S_4\text{'})\}_2]$ and analogous complexes with [FeS]-centers. ("S_4"$^{2-}$ = 1,2-bis(2-mercaptophenylthio)ethane(2-)), *Z. Naturforsch. B 49*, 76−88.
44. Durrant, M. C., (2001) unpublished work.
45. Galindo, A., Hills, A., Hughes, D. L., Richards, R. L., Hughes, M., and Mason, J. (1990) Protonation reactions of dinitrogen complexes of molybdenum and tungsten with PMe_3 as co-ligand. X-ray structure of the hydrazidium complex $[WCl(NNH_3)(PMe_3)_4]\text{-}Cl_2$, *J. Chem. Soc., Dalton Trans.* 283−288.
46. Le Gall, T., Ibrahim, S. K., Gormal, C. A., Smith, B. E., and Pickett, C. J. (1999) The isolated iron−molybdenum cofactor of nitrogenase catalyses hydrogen evolution at high potential, *Chem. Commun.* 773−774.
47. Montet, Y., Amara, P., Volbeda, A., Vernede, X., Hatchikian, E. C., Field, M. J., Frey, M., and Fontecilla-Camps, J. C. (1997) Gas access to the active site of Ni−Fe hydrogenases probed by X-ray crystallography and molecular dynamics, *Nat. Struct. Biol. 4*, 523−526.
48. Mayer, S. M. (2000) X-ray structure determination of Klebsiella pneumoniae nitrogenase component 1, PhD Thesis, pp 149−152, University of East Anglia/John Innes Centre, East Anglia, U.K.
49. Ibrahim, S. K., Vincent, K., Gormal, C. A., Smith, B. E., Best, S. P., and Pickett, C. J. (1999) The isolated iron−molybdenum cofactor of nitrogenase binds carbon monoxide upon electrochemically accessing reduced states, *Chem. Commun.* 1019−1020.
50. George, S. J., Ashby, G. A., Wharton, C. W., and Thorneley, R. N. F. T. (1997) Time-resolved binding of carbon monoxide to nitrogenase monitored by stopped-flow infrared spectroscopy, *J. Am. Chem. Soc.* 6450−6451.
51. Christie, P. D., Lee, H.-I., Cameron, L. M., Hales, B. J., Orme-Johnson, W. H., and Hoffman, B. M. (1996) Identification of the CO-binding cluster in nitrogenase MoFe protein by ENDOR of ^{57}Fe isotopomers, *J. Am. Chem. Soc. 118*, 8707−8709.
52. Shen, J., Dean, D. R., and Newton, W. E. (1997) Evidence for multiple substrate-reduction sites and distinct inhibitor-binding

sites from an altered *Azotobacter vinelandii* nitrogenase MoFe protein, *Biochemistry 36*, 4884−4894.
53. Kim, C.-H., Newton, W. E., and Dean, D. R. (1995) Role of the MoFe protein α-subunit histidine-195 residue in FeMo-cofactor binding and nitrogenase catalysis, *Biochemistry 34*, 2798−2808.
54. Mandon, D., Ott-Woelfel, F., Fischer, J., Weiss, R., Bill, E., and Trautwein, A. X. (1990) Structure and spectroscopic properties of five-coordinate (2-methylimidazolato)- and six-coordinate (imidazole)(imidazolato)iron(II) "picket-fence" porphyrins, *Inorg. Chem. 29*, 2442−2447.
55. Landrum, J. T., Hatano, K., Scheidt, W. R., and Reed, C. A. (1980) Imidazolate complexes of iron and manganese tetraphenylporphyrins, *J. Am. Chem. Soc. 102*, 6729−6735.
56. Nishida, Y., Kino, K., and Kida, S. (1987) Crystal structures of low- and high-spin iron(III) complexes with quadridentate Schiff bases, *J. Chem. Soc., Dalton Trans.* 1157−1161.
57. Winter, J. A., Caruso, D., and Shepherd, R. E. (1988) Influence of pentaamminechromium(III) on the acidity of coordinated imidazoles and pyrazole, *Inorg. Chem. 27*, 1086−1089 and references therein.
58. George, G. N., Prince, R. C., and Bare, R. E. (1996) Electron paramagnetic resonance spectroscopy of the iron−molybdenum cofactor of *Clostridium pasteurianum* nitrogenase, *Inorg. Chem. 35*, 434−438.
59. Lovell, T., Li, J., Case, D. A., and Noodleman, L. (2002) Binding modes for the first coupled electron and proton addition to FeMoco of nitrogenase, *J. Am. Chem. Soc. 124*, 4546−4547.
60. Einsle, O., Tezcan, I. A., Andrade, S. L. A., Schmid, B., Yoshida, M., Howard, J. B., and Rees, D. C. (2002) *Science 297*, 1696−1700.

BI025623Z